

# Bioinspired Adaptive Microdrugs Enhance the Chemotherapy of Malignant Glioma: Beyond Their Nanodrugs

Xuejiao Wang, Xiangrong Hao, Yangning Zhang, Qun Wu, Jiajia Zhou, Zhongman Cheng, Jianping Chen, Sijia Liu, Jiahao Pan, Ying Wang, and Jun-Bing Fan\*

Solid nanoparticle-mediated drug delivery systems are usually confined to nanoscale due to the enhanced permeability and retention effect. However, they remain a great challenge for malignant glioma chemotherapy because of poor drug delivery efficiency and insufficient tumor penetration resulting from the blood–brain barrier/blood–brain tumor barrier (BBB/BBTB). Inspired by biological microparticles (e.g., cells) with excellent adaptive deformation, it is demonstrated that the adaptive microdrugs (even up to 3.0  $\mu\text{m}$  in size) are more efficient than their nanodrugs (less than 200 nm in size) to cross BBB/BBTB and penetrate into tumor tissues, achieving highly efficient chemotherapy of malignant glioma. The distinct delivery of the adaptive microdrugs is mainly attributed to the enhanced interfacial binding and endocytosis via adaptive deformation. As expected, the obtained adaptive microdrugs exhibit enhanced accumulation, deep penetration, and cellular internalization into tumor tissues in comparison with nanodrugs, significantly improving the survival rate of glioblastoma mice. It is believed that the bioinspired adaptive microdrugs enable them to efficiently cross physiological barriers and deeply penetrate tumor tissues for drug delivery, providing an avenue for the treatment of solid tumors.

## 1. Introduction

Glioma is recognized as one of the most aggressive and malignant tumors due to the high infiltration and invasion capabilities of glioma cells.<sup>[1,2]</sup> The treatment of glioma has been hindered by limited clinical outcomes, attributed to the poor drug delivery efficiency and inadequate tumor penetration resulting from BBB/BBTB.<sup>[3–5]</sup> To address these challenges, numerous studies have focused on solid nanoparticle-mediated drug delivery systems to improve the efficacy of chemotherapeutic drugs.<sup>[6–8]</sup> In designing these systems, a central dogma is to minimize nanoparticle size as small as possible. Based on the physiological structures of BBB, nanoparticles with sizes between 20 and 70 nm have been identified as optimal for penetrating the tumor microenvironments.<sup>[9–11]</sup> To further augment their ability to cross the BBB/BBTB, these nanoparticles are often functionalized with biomolecules, such as cell-penetrating peptides or BBB-targeting ligands.<sup>[12–15]</sup> However,

even under these stringent conditions, the effectiveness of solid nanoparticle-mediated drug delivery systems for glioma treatment remains constrained.<sup>[16–18]</sup>

The BBB/BBTB primarily consists of endothelial cells with tight junctions, pericytes, astrocytic endfeet, and tumor cells.<sup>[19]</sup> To improve the crossing of the BBB/BBTB, the underlying science of drug delivery systems remains to regulate the interaction between drug particles and cells, such as enhancing their interfacial binding, endocytosis, and transcytosis. Therefore, there is an imperative need for new efficient solutions to further amplify the interaction to enhance the crossing of the BBB/BBTB. In living systems, biological microparticles, such as cells, with sizes even larger than 10  $\mu\text{m}$ , have the ability to transport a significant amount of cargo and traverse various physiological barriers with ease.<sup>[20–23]</sup> This phenomenon raises profound questions: how do these micro-sized microparticles possess the capability to cross such barriers freely? The answer appears to be their exceptional adaptive deformation capacities, which allow them to deform multiple times to navigate through diverse physiological barriers, beyond molecular recognition. Furthermore,

X. Wang, X. Hao, Y. Zhang, Q. Wu, Z. Cheng, J. Chen, S. Liu, J. Pan, Y. Wang, J.-B. Fan

Cancer Research Institute  
 Experimental Education/Administration Center  
 School of Basic Medical Sciences  
 Southern Medical University  
 Guangzhou 510515, P. R. China  
 E-mail: [fjb2012@mail.ipc.ac.cn](mailto:fjb2012@mail.ipc.ac.cn)

J. Zhou  
 South China Advanced Institute for Soft Matter Science and Technology  
 School of Emergent Soft Matter  
 South China University of Technology  
 Guangzhou 510515, P. R. China

J. Chen  
 Department of Radiotherapy  
 The Sixth Affiliated Hospital of Guangzhou Medical University  
 Qingyuan People's Hospital  
 Qingyuan 511518, P. R. China

 The ORCID identification number(s) for the author(s) of this article can be found under <https://doi.org/10.1002/adma.202405165>

DOI: 10.1002/adma.202405165

these adaptive deformation capacities facilitate cell-to-cell communication by increasing their contact interfaces.<sup>[24–26]</sup> Inspired by this living phenomenon, the concept of adaptive deformation may provide an alternative solution for drug delivery systems to further amplify the interaction between drug particles and cells (such as endothelial cells and tumor cells). Due to the increase in contact interfaces resulting from adaptive deformation, there is potential for enhanced interfacial binding and downstream endocytosis, which is beneficial to improving the crossing of the BBB/BBTB.

Herein, inspired by the biological microparticles with excellent adaptive deformation capacity, we demonstrated that micro-sized microdrugs could efficiently cross BBB/BBTB when endowed with good adaptive deformation capacity. Different from the traditional concept, we found that the adaptive microdrugs were more efficient than their nanodrugs in bringing drugs into the glioblastoma tissues, allowing efficient accumulation, deep penetration, and cellular internalization, thus greatly enhancing the anti-tumor efficacy of malignant glioma. In our design, we used cross-linkable methoxy polyethylene glycol-sodium alginate to fabricate adaptive drug particles, as proof of concept.<sup>[27–30]</sup> Briefly, methoxy polyethylene glycol (mPEG)-oxidized sodium alginate (mPEG-OXA) was firstly mixed with DOX, which was then crosslinked to fabricate the adaptive drug particles in the presence of CaCl<sub>2</sub> under shearing. Subsequently, the obtained adaptive drug particles were further modified with c(RGDyK) peptide (capable of binding with integrin  $\alpha v\beta 3$  receptor expressed in neovascular endothelial cells and glioma cells).<sup>[31–35]</sup> During the process of drug delivery, the receptor–ligand interaction provided the first driving force to achieve interfacial binding between adaptive drug particles and cells. Subsequently, adaptive deformation of the drug particles played its role in efficiently crossing BBB/BBTB by adaptive deformation-mediated endocytosis. In the downstream, they also exhibited excellent transcytosis capacity to allow deep penetration into tumor tissues. Therefore, adaptive deformation-enhanced receptor-ligand-interfacial binding and endocytosis were the main contributions to the enhancement of BBB/BBTB crossing and tumor tissue penetration of adaptive drug particles. Owing to the more powerful binding capacity of microdrugs with cells, the adaptive microdrugs exhibited more efficient drug delivery capacity and were able to carry more drugs into cells than their nanodrugs. In addition, some adaptive microdrugs and nanodrugs may also cross BBB/BBTB due to leakage, which occurs as a consequence of the broken integrity of the BBB during the progression of glioma. As expected, the enhanced accumulation, penetration, and cellular internalization of the adaptive microdrugs would be achieved, significantly promoting the chemotherapy efficiency of malignant glioma (Figure 1).

## 2. Results and Discussion

### 2.1. Synthesis, Characterization, and Biological Activities of the Bioinspired Adaptive Nanodrugs and Adaptive Microdrugs In Vitro

The bioinspired adaptive drug particles (including adaptive nanodrugs and adaptive microdrugs) were fabricated by crosslinking DOX@mPEG-OXA under shearing and then modified with

c(RGDyK). In brief, mPEG-NH<sub>2</sub> was initially reacted with OSA-COOH through an amidation reaction to produce mPEG-OXA. Subsequently, DOX was encapsulated into the mPEG-OXA using Ca<sup>2+</sup> crosslinking under shear conditions, resulting in the creation of DOX@mPEG-OXA drug particles. These particles were then further modified with c(RGDyK) via a reaction between the residual carboxyl groups of the OSA in mPEG-OXA and the amino groups of c(RGDyK). Consequently, the bioinspired adaptive drug particles could be fabricated. In our study, we defined that the adaptive drug particles with a size of more than 0.5  $\mu\text{m}$  were adaptive microdrugs (AMD), while those with a size of less than 0.5  $\mu\text{m}$  were adaptive nanodrugs (AND). The optimal molar ratio of mPEG and the alginate units in OSA in fabricating adaptive particles was 1:10, as indicated by the cellular uptake and antiproliferation in GL261 cells (Figures S1 and S2, Supporting Information). The composition of mPEG-OXA-c(RGDyK) was confirmed by <sup>1</sup>H NMR and FTIR spectra (Figure S3, Supporting Information).<sup>[36–41]</sup> As shown in Figure 2A, adaptive drug particles with different sizes from  $0.12 \pm 0.03$  to  $3.25 \pm 0.12 \mu\text{m}$  were fabricated by adjusting the shear velocity, as indicated by dynamic light scattering (DLS) (Figure 2A,B; Figure S4 and Table S1, Supporting Information). Transmission electron microscopy (TEM) images showed that the sizes of these adaptive drug particles were approximately shrunk in half after dehydration (Figure 2B,C; Figure S5, Supporting Information). In addition, the stability of adaptive nanodrugs and microdrugs in 50% FBS condition was evaluated. The results from DLS analysis indicated that the stability of these adaptive nanodrugs and microdrugs was excellent when maintained in a 50% FBS environment (Figure S6, Supporting Information). Furthermore, we assessed their stability in mouse blood after intravenous administration at intervals of 0.5, 3, 6, 12, and 24 h. DLS results indicated that the sizes of adaptive nanodrugs and microdrugs nearly had no changes over the period from 0.5 to 24 h (Figure S7, Supporting Information). In addition, TEM images demonstrated that these adaptive microdrugs (AMD-0.8  $\mu\text{m}$ ) adsorbed a minimal quantity of proteins in blood after 0.5, 3, 6, 12, and 24 h of intravenous injection, yet maintained their original morphologies and monodispersity across different time points (Figure S8A, Supporting Information). When these adaptive drug particles were delivered into glioma tissues, they exhibited nearly unchanged morphologies (Figure S8B, Supporting Information). These results indicated that the adaptive nanodrugs and microdrugs had excellent stability and were resistant to disintegration in blood post-intravenous injection. UV-vis spectra revealed that the adaptive drug particles had obvious absorption peaks of DOX at 480 nm, indicating that DOX was successfully encapsulated (Figure S9, Supporting Information). The encapsulation efficiency and loading efficiency of DOX are shown in Table S2 (Supporting Information).

We first explored the entry mode of these adaptive drug particles with different sizes in bEnd.3 and GL261 cells in the presence of endocytic inhibitors (Figure S10, Supporting Information). In bEnd.3 cells, the nanodrugs of AND-0.1  $\mu\text{m}$ , AND-0.2  $\mu\text{m}$ , AND-0.4  $\mu\text{m}$  proceeded with clathrin-mediated endocytosis and caveolin-mediated endocytosis. Microdrugs of AMD-0.8  $\mu\text{m}$  proceeded with both clathrin-mediated and caveolin-mediated endocytosis; whereas the cellular uptake of AMD-1.5  $\mu\text{m}$  and AMD-3.0  $\mu\text{m}$  were mainly proceeded with

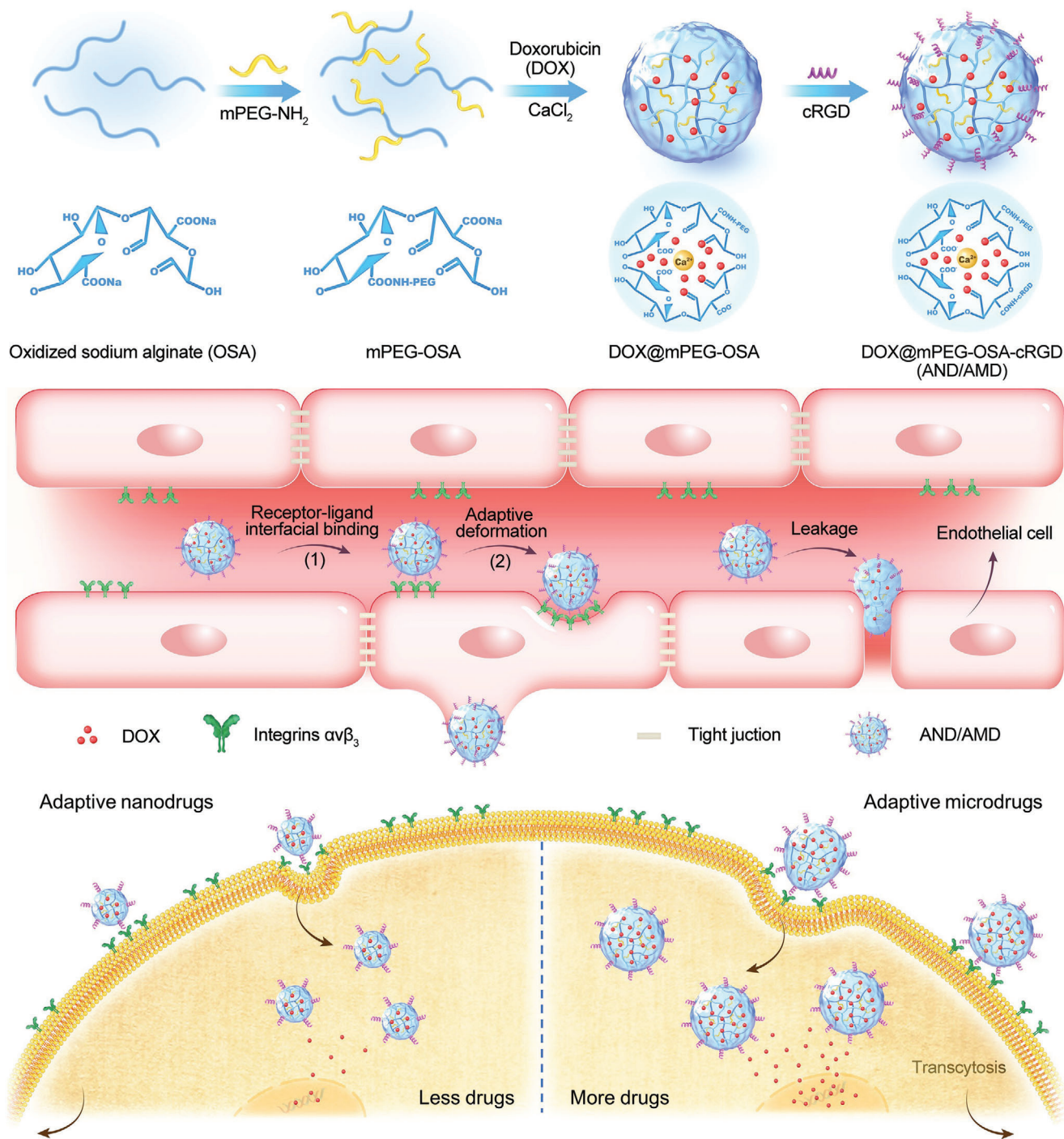


**Figure 1.** Schematic illustration of the bioinspired adaptive nanodrugs and microdrugs for the treatment of malignant glioma. The bioinspired adaptive drug particles (including adaptive nanodrugs and adaptive microdrugs) were fabricated by crosslinking doxorubicin (DOX) loaded methoxy polyethylene glycol (mPEG)-oxidized sodium alginate (mPEG-OSA) under high-speed shearing and then modified with c(RGDyK). The obtained adaptive drug particles could first be interfacially bound through the interaction between c(RGDyK) and integrin  $\alpha v \beta_3$  receptor in neovascular endothelial and glioma cells. Subsequently, these bound adaptive drug particles enabled them to deform to efficiently cross BBB/BBTB by adaptive deformation-enhanced endocytosis. Owing to more powerful binding capacity of microdrugs with cells, the adaptive microdrugs exhibited more efficient drug delivery capacity and were able to carry more drugs into cells than their nanodrugs. In addition, some adaptive microdrugs and nanodrugs may also cross BBB/BBTB due to leakage as a result of BBB dysfunction. Thus, micro-sized microdrugs could also efficiently cross BBB/BBTB and penetrate into tumor tissues when endowed with good adaptive deformation capacity, allowing the enhanced accumulation, deep penetration, and cellular internalization into tumor tissues in comparison with nanodrugs.

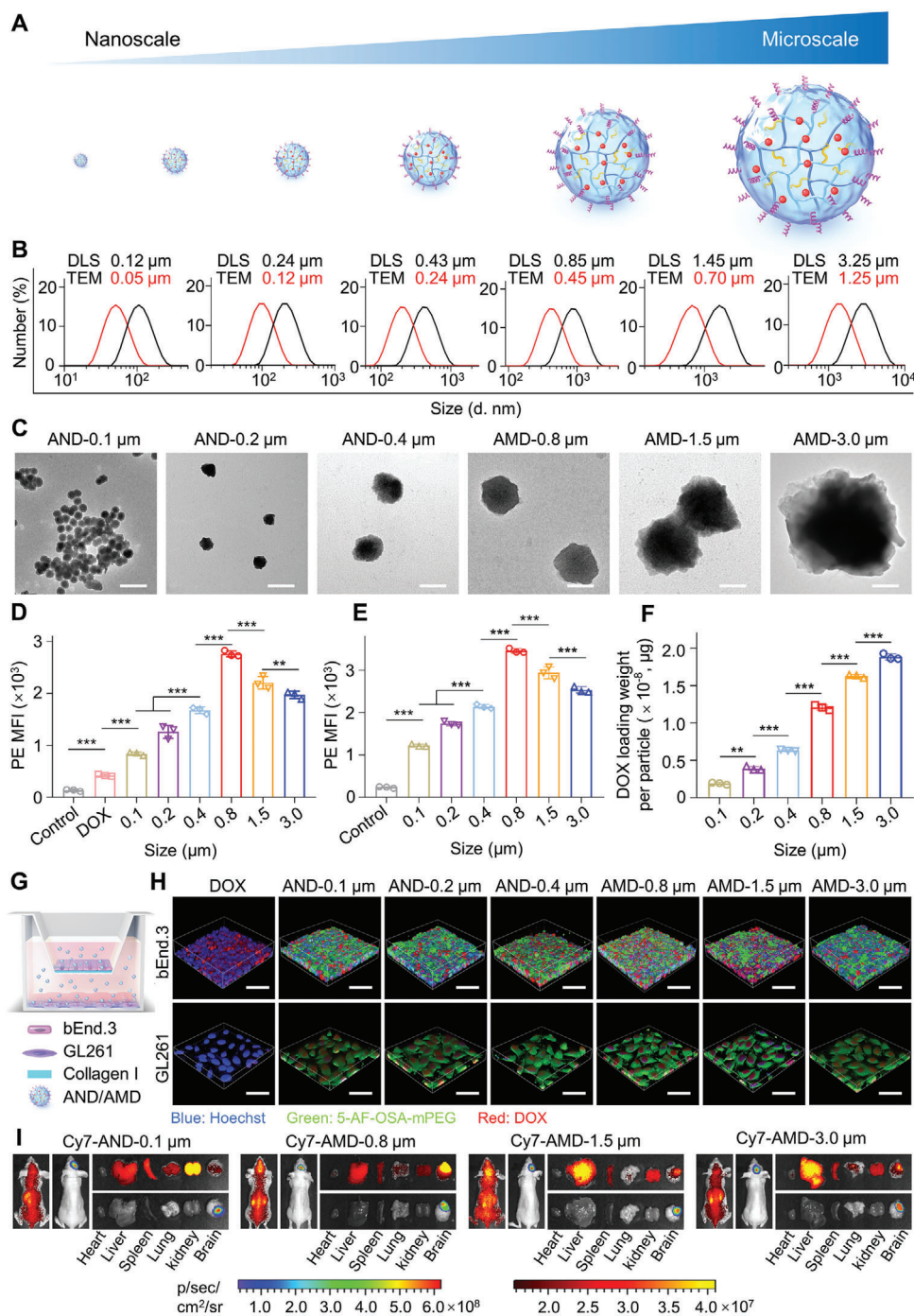


**Figure 2.** Synthesis, characterization and biological activities of the bioinspired adaptive nanodrugs and microdrugs. A) Schematic illustration of the obtained adaptive nanodrugs and microdrugs with different sizes. B) The sizes of the obtained adaptive nanodrugs and microdrugs in swelling and shrinking states. TEM images showed the sizes of these adaptive nanodrugs and microdrugs were approximately shrunk in half after dehydration. C) TEM images of the obtained adaptive nanodrugs and microdrugs with different sizes. Scale bars in the three images on the left: 200 nm; Scale bars in the three images on the right: 300 nm. D) The cellular uptake of DOX within adaptive nanodrugs and microdrugs in GL261 cells quantified by the same dose of DOX ( $2.5 \mu\text{g mL}^{-1}$ ), as detected by flow cytometry. E) The cellular uptake of DOX within adaptive nanodrugs and microdrugs in GL261 cells quantified by the same particle number ( $8 \times 10^{12}$  particles  $\text{mL}^{-1}$ ), as detected by flow cytometry. The results indicated that the adaptive microdrugs had more efficient internalization capacity than that of their nanodrugs. F) The DOX loading weight per particle with different sizes. G) Schematic illustration of the in vitro BBB model constructed by bEnd.3 and GL261 cells. H) Confocal 3D images of the adaptive nanodrugs and microdrugs crossing BBB in the in vitro BBB model. In addition to nanodrugs, microdrugs with approximate sizes of 1.5 and 3.0  $\mu\text{m}$  also effectively traversed the BBB. Scale bars: 50  $\mu\text{m}$ . I) In vivo fluorescence images of orthotopic intracranial GL261-luc glioma mice at 96 h after administration of Cy7-AND-0.1  $\mu\text{m}$ , Cy7-AMD-0.8  $\mu\text{m}$ , Cy7-AMD-1.5  $\mu\text{m}$ , and Cy7-AMD-3.0  $\mu\text{m}$ . Results are represented as mean  $\pm$  SD ( $n = 3$ ),  $*P < 0.05$ ,  $**P < 0.01$ ,  $***P < 0.001$ .

macropinocytosis. Similar results were also observed in GL261 cells. The results indicated that these adaptive drug particles with different sizes enabled entry into cells through different pathways. Next, the cellular uptake of DOX and adaptive drug particles with different sizes were detected by Flow cytometry in GL261 cells. We used the same dosage of DOX within adaptive drug particles or the same number of adaptive drug particles to compare the cellular uptake of DOX within adaptive nanodrugs and adaptive microdrugs, respectively. The results showed that the adaptive microdrugs (AMD-0.8  $\mu\text{m}$ , AMD-1.5  $\mu\text{m}$ ) exhibited more efficient internalization capacity than that of their nanodrugs (AND-0.1  $\mu\text{m}$ , AND-0.2  $\mu\text{m}$ ). Among them, AMD-0.8  $\mu\text{m}$  showed the best internalization capacity. In these internalized particles, the intracellular uptake of DOX in AMD-0.8  $\mu\text{m}$  was  $\approx 3.2$ -fold higher than in AND-0.1  $\mu\text{m}$  and 2.1-fold higher than in AND-0.2  $\mu\text{m}$ . The order of intracellular uptake of DOX in internalized particles was: AMD-0.8  $\mu\text{m}$  > AMD-1.5  $\mu\text{m}$  > AMD-3.0  $\mu\text{m}$  > AND-0.4  $\mu\text{m}$  > AND-0.2  $\mu\text{m}$  > AND-0.1  $\mu\text{m}$  (Figure 2D,E). To investigate why these adaptive microdrugs were more efficient than their nanodrugs in internalization, we detected the DOX loading weight in one particle by nanoparticle tracking analysis (NTA) and UV-vis. The results indicated that the DOX loading weight in one particle increased with an increase of particle size (Figure 2F). These results demonstrated that adaptive microdrugs were able to carry more drugs into cells than their nanodrugs because of greater drug loading capacity. In other words, one adaptive microdrug was comparable to several nanodrugs in bringing drugs into a cell.

## 2.2. The Crossing BBB Capacity and Antitumor Efficacy of Adaptive Nanodrugs and Adaptive Microdrugs In Vitro and In Vivo

To evaluate the BBB-crossing capacity of the adaptive drug particles with different sizes, we constructed an in vitro BBB model using bEnd.3 and GL261 cells. The bEnd.3 cells were seeded and cultured on collagen I in the upper transwell chamber, while GL261 cells were seeded and cultured on a coverslip in the lower chamber (Figure 2G). The expression of ZO-1, Claudin-1, and PECAM-1 proved that the in vitro BBB model was successfully constructed (Figure S11, Supporting Information). The results indicated that these adaptive drug particles with different sizes crossed the in vitro BBB from bEnd.3 cells to downstream GL261 cells more efficient than DOX (Figure 2H; Figure S12, Supporting Information). In addition, the adaptive microdrugs, even with sizes of  $\approx 1.5$  and 3.0  $\mu\text{m}$ , also crossed the BBB efficiently. To further confirm these capacities in vivo, we investigated the tumor targeting and BBB-crossing capacity of Cy7-labeled adaptive drug particles with different sizes in nude mice bearing intracranial GL261-Luc tumors via intravenous injection (Figure S13, Supporting Information). Real-time images of biodistributions of free Cy7 and Cy7-labeled adaptive nanodrugs and microdrugs with different sizes were observed at different times after administration, through which the tumors were monitored by the bioluminescence of GL261-Luc cells (Figure S13A, Supporting Information). Mice were sacrificed at 96 h, and the major organs (heart, liver, spleen, lung, kidney, and brain) were excised for comparison of drug accumulation by perfusion. The

results showed that these adaptive nanodrugs and microdrugs were mainly distributed in the liver, kidney, spleen, and tumor (Figure 2I; Figure S13B, Supporting Information). The Cy7-AMD-0.8  $\mu\text{m}$  exhibited the highest accumulation in the tumor, suggesting that they possessed the best capacity to cross BBB and target glioma tissues. Moreover, we observed that Cy7-AMD-1.5  $\mu\text{m}$  and Cy7-AMD-3.0  $\mu\text{m}$  could also cross BBB and efficiently accumulate in tumor tissues.

We next assessed the anti-glioma efficacy of PBS, DOX, and the obtained adaptive drug particles with different sizes in the orthotopic GL261-Luc glioblastoma xenograft mice (Figure 3A). The results indicated that the adaptive microdrugs, even with a size of  $\approx 0.8$ , 1.5, and 3.0  $\mu\text{m}$  could also cross the BBB to achieve therapeutic effects on gliomas. As expected, they exhibited more efficient anti-glioma efficacy than their nanodrugs. In particular, the AMD-0.8  $\mu\text{m}$  group presented the best anti-glioma efficacy in comparison with the other treatment groups (Figure 3B,C; Figure S14, Supporting Information). The order of median survival time was: AMD-0.8  $\mu\text{m}$  (66 d) > AMD-1.5  $\mu\text{m}$  (54 d) > AMD-3.0  $\mu\text{m}$  (46 d) > AND-0.4  $\mu\text{m}$  (38 d) > AND-0.1  $\mu\text{m}$  (35 d) > AND-0.2  $\mu\text{m}$  (34 d) > DOX (27 d) and PBS (24 d). Furthermore, we performed immunohistochemical analyses of Ki67 and CD34, which are markers of cell proliferation and endothelial-lined blood vessels, respectively (Figure 3D). The expression levels of Ki67 and CD34 in each group were as follows: PBS > DOX > AND-0.2  $\mu\text{m}$  > AND-0.1  $\mu\text{m}$  > AND-0.4  $\mu\text{m}$  > AMD-3.0  $\mu\text{m}$  > AMD-1.5  $\mu\text{m}$  > AMD-0.8  $\mu\text{m}$  (Figure S15, Supporting Information). These results suggested that micro-sized adaptive microdrugs (AMD-0.8  $\mu\text{m}$ , AMD-1.5  $\mu\text{m}$ , and AMD-3.0  $\mu\text{m}$ ) could cross the BBB to penetrate into tumor tissues and exhibited more efficient capacity than their nanodrugs (AND-0.1  $\mu\text{m}$ , AND-0.2  $\mu\text{m}$ , and AND-0.4  $\mu\text{m}$ ) to suppress the growth of glioma.

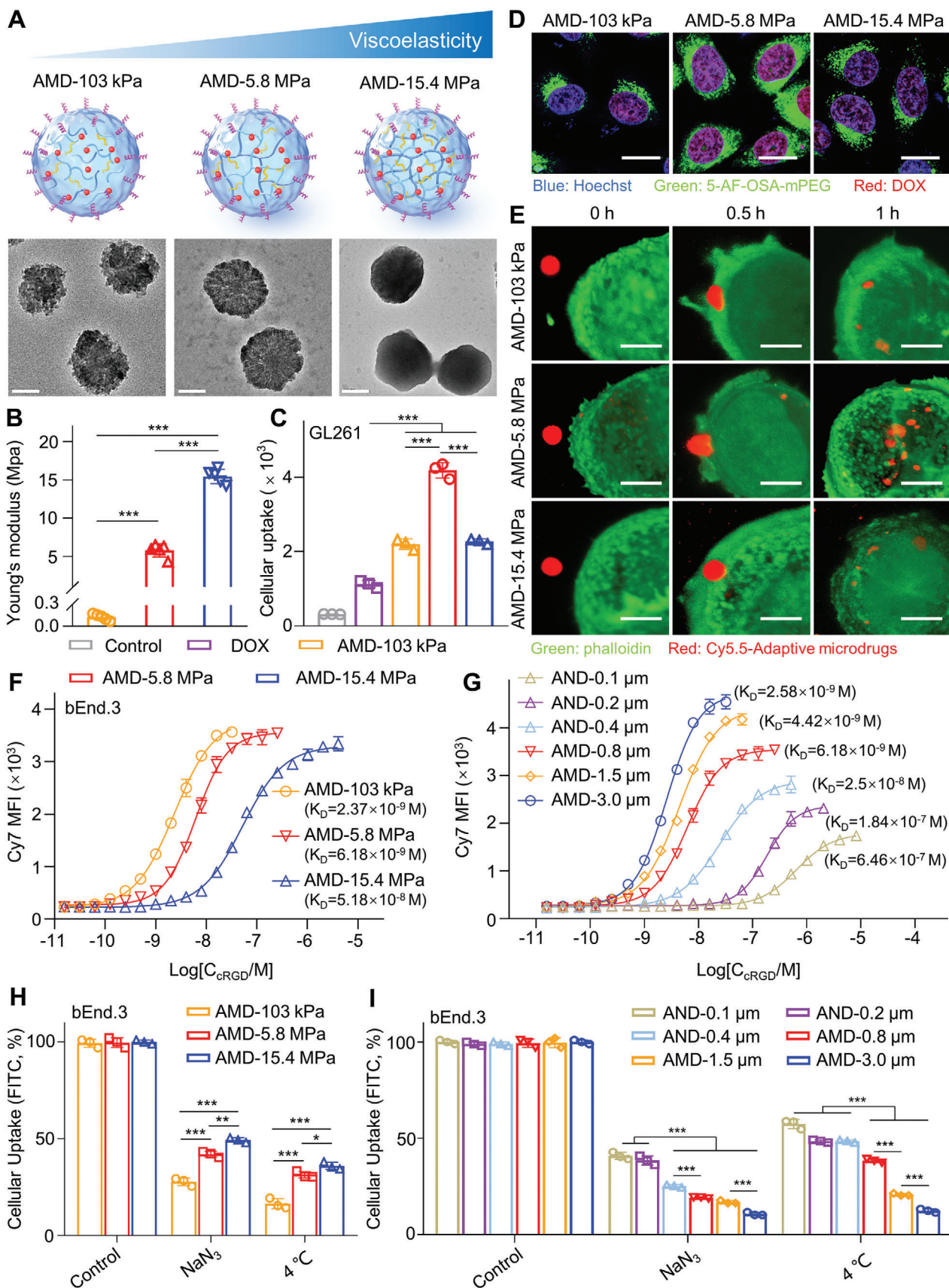
## 2.3. The Mechanism of Adaptive Microdrugs on Crossing BBB/BBTB for Enhanced Glioma Chemotherapy

We have proposed that, like natural biological microparticles (e.g., cells), the adaptive deformation capacity of these micro-sized microdrugs may play a key role in crossing BBB/BBTB for efficient drug delivery and downstream glioma chemotherapy.

### 2.3.1. Fabrication of the Three Kinds of Adaptive Microdrugs with Different Viscoelasticities

To verify our proposal, three kinds of adaptive microdrugs (AMD-103 kPa, AMD-5.8 MPa, and AMD-15.4 MPa) with similar hydrodynamic diameters (approximately 0.85  $\mu\text{m}$ ) but different viscoelasticities were controllably fabricated by adjusting the concentration of  $\text{CaCl}_2$  (Figure 4A; Figure S16 and Table S3, Supporting Information). The viscoelasticity of these adaptive microdrugs was determined by atomic force microscopy (AFM) and the results demonstrated that the elastic modulus of the obtained adaptive microdrugs was increased with the increase of the concentration of  $\text{CaCl}_2$  (Figure 4B; Figure S17, Supporting Information). Accordingly, their modulus were  $103 \pm 0.04$  kPa (AMD-103 kPa),  $5.8 \pm 0.31$  MPa (AMD-5.8 MPa), and  $15.4 \pm 0.23$  MPa (AMD-15.4 MPa), respectively. Moreover, to investigate the stability of obtained adaptive microdrugs, we selected 50% fetal bovine





serum (FBS) solution to mimic blood conditions, and the result showed the size and polydispersity index (PDI) of the obtained adaptive microdrugs (AMD-103 kPa, AMD-5.8 MPa, and AMD-15.4 MPa) did not change significantly within 168 h, indicating their excellent stability (Figure S18, Supporting Information). Moreover, the obtained adaptive microdrugs exhibited good pH-responsive drug release due to the imine bond formed by the aldehyde of OSA and amino of DOX (Figure S19, Supporting Information).<sup>[42,43]</sup> These results demonstrated that the bioinspired adaptive microdrugs with controllable viscoelasticities could be successfully fabricated.

### 2.3.2. The Biological Activities of the Three Kinds of Adaptive Microdrugs with Different Viscoelasticities In Vitro

We investigated the in vitro biological activities of the three kinds of adaptive microdrugs (AMD-103 kPa, AMD-5.8 MPa, and AMD-15.4 MPa). Glioma cells LN229, GL261, U251, human cerebral microvascular endothelial bEnd.3 cells with positive expression of  $\alpha v\beta 3$  integrins, and normal glial HEB cells with negative control were selected to investigate the biological activities of adaptive microdrugs in vitro (Figure S20, Supporting Information). The cellular uptake results indicated that the three kinds of adaptive microdrugs modified with c(RGDyK) could significantly enhance the uptake of  $\alpha v\beta 3$ -positive GL261 and bEnd.3 cells compared to those without modification, confirming the effect of receptor–ligand binding on the particle–cell interaction (Figure S21, Supporting Information). Compared to free DOX, the three kinds of adaptive microdrugs (modified with c(RGDyK)), especially the AMD-5.8 MPa, showed excellent internalization capacity in GL261, LN229, U251, and HEB cells (Figure 4C; Figure S22, Supporting Information). Meanwhile, we used a laser scanning confocal microscope to observe the cellular uptake of DOX and 5-amino fluorescein-labeled adaptive microdrugs in GL261 cells. The results showed that the adaptive microcarrier of mPEG-OA (labeled with 5-amino fluorescein) with green fluorescence was mainly located in the cytoplasm, while the loaded DOX with red fluorescence was observed in the nucleus. Among these microparticles, AMD-5.8 MPa exhibited much higher cellular uptake than other groups (free DOX, AMD-103 kPa, and AMD-15.4 MPa) (Figure 4D; Figure S23, Supporting Information). Similar results were also observed in U251 cells (Figure S24, Supporting Information). Accordingly, AMD-5.8 MPa exhibited the best

antiproliferation in GL261 and LN229 cells. While the adaptive microcarrier of mPEG-OA had no obvious cytotoxicity (Figure S25 and Table S4, Supporting Information). Furthermore, we compared the penetration ability of AMD-5.8 MPa and free DOX in multicellular GL261 spheroids (Figure S26, Supporting Information). The results indicated that the penetration capacity of adaptive microdrugs (AMD-5.8 MPa) significantly surpassed that of free DOX, indicating their superior penetration within multicellular tumor spheroids.

Subsequently, we observed the interfacial interaction between the adaptive microdrugs and GL261 cells. When the three kinds of spherical adaptive microdrugs arrived on the surface of GL261 cells, an obvious viscoelastic deformation could be observed, respectively. Interestingly, the three kinds of spherical adaptive microdrugs showed different entrances into the GL261 cells. The AMD-103 kPa deformed into an excessive shape (oblate), while the AMD-5.8 MPa deformed into a prolate ellipsoid. By contrast, the AMD-15.4 MPa only deformed slightly due to its higher modulus (Figure 4E). These results indicated that the adaptive deformation of microdrugs played a critical role in the intracellular uptake; however, it is not that softer microdrugs were more easily taken up by cells. We investigated the binding capacity of receptor–ligand between adaptive microdrugs and  $\alpha v\beta 3$ -positive bEnd.3 cells. The receptor–ligand binding between adaptive microdrugs and bEnd.3 cells enabled to reduction of the intracellular free energy, which drove the membrane wrapping for microdrug internalization.<sup>[44]</sup> The dissociation constant  $K_D$  of the adaptive microdrugs was calculated by dynamic equilibrium assay.<sup>[45,46]</sup> As shown in Figure 4F, the  $K_D$  of the three kinds of adaptive microdrugs with different viscoelasticities increased with increasing the modulus. Also, the  $K_D$  was highly dependent on the size of adaptive drug particles. These results indicated that more efficient deformation or larger particle size was, the lower  $K_D$  was, indicating a more powerful binding capacity of microdrugs with cells than their nanodrugs (Figure 4G).

$$K_D = \frac{[R]_f [L]_f}{[RL]} \quad (1)$$

$[R]_f$  is the concentration of free R (receptor),  $[L]_f$  is the concentration of free L (ligand), and  $[RL]$  is the concentration of receptor–ligand complex.

**Figure 4.** The mechanism of adaptive microdrugs with different viscoelasticities to cross BBB/BBTB for efficient glioma chemotherapy. A) Schematic illustration and TEM images of the obtained adaptive microdrugs. Three kinds of adaptive microdrugs with similar sizes but different viscoelasticities could be controllably fabricated. Scale bars: 200 nm. B) The Young's modulus of the obtained adaptive microdrugs. The Young's modulus of these adaptive microdrugs was  $103 \pm 0.04$  kPa (AMD-103 kPa),  $5.8 \pm 0.31$  MPa (AMD-5.8 MPa), and  $15.4 \pm 0.23$  MPa (AMD-15.4 MPa), respectively. C) Flow cytometry detection of the cellular uptake of DOX and adaptive microdrugs in GL261 cells. D) Laser scanning confocal microscope images of the intracellular localization of 5-amino fluorescein-labeled adaptive microdrugs in GL261 cells. Scale bars: 20  $\mu$ m. Compared to free DOX, the three kinds of adaptive microdrugs, especially the AMD-5.8 MPa, exhibited more efficient internalization capacity. E) The process of the endocytosis of AMD-103 kPa, AMD-5.8 MPa, and AMD-15.4 MPa in GL261 cells. Membrane actin and adaptive microdrugs were labeled by phalloidin (green) and Cyanine5.5 (red), respectively. Scale bars: 2  $\mu$ m. The AMD-103 kPa deformed into an excessive shape (oblate), while the AMD-5.8 MPa deformed into a prolate ellipsoid. By contrast, the AMD-15.4 MPa only deformed slightly due to its higher modulus. F,G) Binding capacity analysis. Effect of dissociation constant  $K_D$  for different-viscoelastic or different-sized adaptive drug particles. The results indicated that more efficient deformation or larger particle size was, the lower  $K_D$  was, indicating a more powerful binding capacity of microdrugs with cells than their nanodrugs. H,I) Effects of temperature and mitochondrial inhibitor sodium azide (NaN<sub>3</sub>) on adaptive microdrugs with various viscoelasticities or sizes intracellular uptake in bEnd.3 cells. The results suggested that although the excessive deformation or larger particle size could enhance the multivalent binding between adaptive microdrugs and cells due to the increase of their contact areas, softer particles (AMD-103 kPa) or larger particles (such as AMD-3.0  $\mu$ m) required more energy for membrane wrapping. Results are represented as mean  $\pm$  SD ( $n = 3$ ). \* $P < 0.05$ , \*\* $P < 0.01$ , \*\*\* $P < 0.001$ .

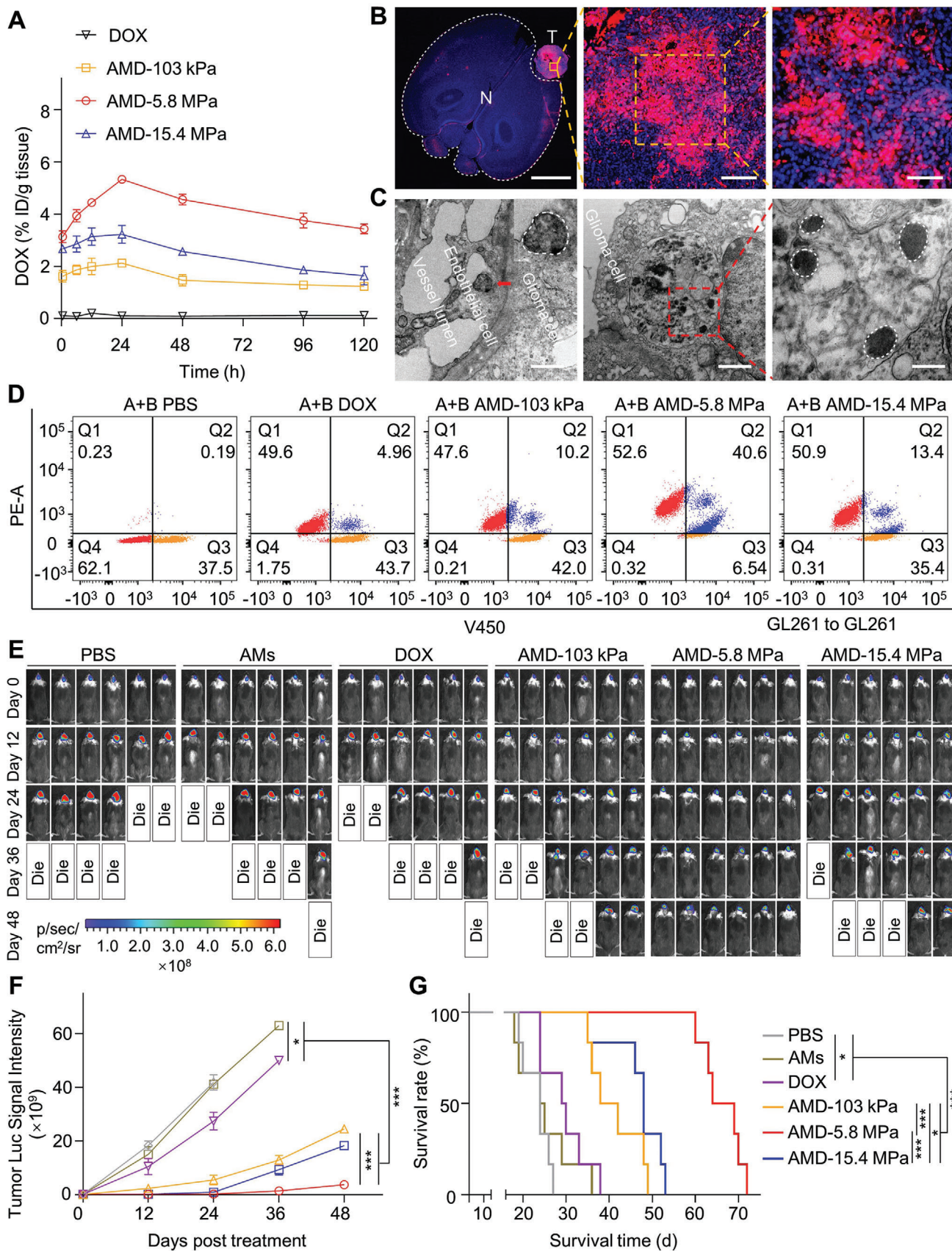
Furthermore, we tested the energy expenditure of internalizing the adaptive nanodrugs and microdrugs in bEnd.3 and GL261 cells by treating them with 4 °C or mitochondrial ATP inhibitor (NaN<sub>3</sub>), respectively. The results indicated that when cells were incubated at 4 °C or treated with NaN<sub>3</sub>, the internalization capacity of the three kinds of viscoelastic microdrugs, especially the AMD-103 kPa, was dramatically decreased. The result suggested that softer microparticles (AMD-103 kPa) needed much more energy for membrane wrapping than the AMD-5.8 MPa and AMD-15.4 MPa during the cellular internalization process (Figure 4H; Figure S27, Supporting Information). In addition, adaptive microdrugs needed much more energy for cellular internalization than those nanodrugs, especially the AMD-1.5 μm and AMD-3.0 μm (Figure 4I; Figure S28, Supporting Information). The above results suggested that although the excessive deformation or larger particle size could enhance the multivalent binding between adaptive microdrugs and cells due to the increase of their contact interfaces, softer particles (AMD-103 kPa) or larger particles (such as AMD-3.0 μm) required more energy for membrane wrapping to proceed the downstream endocytosis.<sup>[47]</sup> Therefore, we may conclude that moderate deformation and size of adaptive microdrugs (such as AMD-0.8 μm with a modulus of 5.8 mPa) are essential for crossing BBB/BBTB. In these adaptive microdrugs, the multivalent interfacial binding and endocytosis-associated energy consumption may reach a state of maximum equilibrium. This results in a more efficient crossing of the BBB/BBTB compared to other adaptive drug particles.

### 2.3.3. The Biological Activities of the Three Kinds of Adaptive Microdrugs with Different Viscoelasticities In Vivo

Next, the in vivo biodistribution and tumor-targeting capacity of Cy7-labeled adaptive microdrugs were investigated. We first detected the retention of Cy7 and Cy7-labeled adaptive microdrugs with different viscoelasticities in the blood of SD rats. The results indicated that the fluorescent signal of Cy7-AMD-5.8 MPa was stronger than that of Cy7, Cy7-AMD-103 kPa, and Cy7-AMD-15.4 MPa, even after 120 h (Figure S29, Supporting Information). Subsequently, we measured the DOX concentration in the plasma of SD rats at different times after intravenous injection of DOX, AMD-103 kPa, AMD-5.8 MPa, and AMD-15.4 MPa. The results indicated that the maximum concentration and half-life of DOX in AMD-5.8 MPa were significantly higher than that in free DOX, AMD-103 kPa, and AMD-15.4 MPa (Figure S30 and Table S5, Supporting Information). Next, we detected the accumulation of the three kinds of adaptive microdrugs in tumors. The Cy7-AMD-5.8 MPa exhibited the highest accumulation in tumors, which was 27, 5.8, and 3.5 times as high as the Cy7, Cy7-AMD-103 kPa, and Cy7-AMD-15.4 MPa, respectively (Figure S31, Supporting Information), suggesting that Cy7-AMD-5.8 MPa possessed the best capacity to cross BBB and target glioma tissues. Furthermore, we detected the DOX concentration in organs at 1, 6, and 24 h after intravenous administration of free DOX and the three kinds of adaptive microdrugs (AMD-103 kPa, AMD-5.8 MPa, and AMD-15.4 MPa). It was found that the DOX accumulation of adaptive microdrugs (AMD-103 kPa (2.13% ± 0.30%), AMD-5.8 MPa (5.43% ± 0.36%), and AMD-15.4 MPa (3.23% ± 0.18%)) in tumor tissues at 24 h were significantly

higher than that in the free DOX group (0.11% ± 0.06%), especially in AMD-5.8 MPa (Figure S32, Supporting Information). As time extended to 120 h, the drug delivery efficiency of AMD-5.8 MPa remained stable at 3.8% ± 0.07% (Figure 5A). We investigated the interaction between the reticuloendothelial system and adaptive microdrugs by measuring the cellular uptake of adaptive microdrugs in RAW264.7 (Figure S33, Supporting Information). The results indicated that the cellular uptake of these adaptive microdrugs in RAW264.7 was increased with the increase of modulus, indicating that immune systems may tend to phagocytize more stiffness particles, which is consistent with the results of previous reports.<sup>[48–50]</sup> It was widely recognized that the interfacial interaction between drug delivery systems and cells significantly influences their fates, including transport, metabolism, and distribution. Aside from deformation, strategies such as multiple ligand synergistic modification (utilizing angiopep-2 peptide, ApoE peptide, transferrin, and so on), autologous cell/tissue-derived active biomaterials as delivery vehicles (extracellular vesicles, extracellular matrix hydrogel) or employing cell membrane camouflage may offer an alternative approach to further enhance drug delivery efficiency in tumor tissues.

In addition, we detected the accumulation of AMD-5.8 MPa in intracranial GL261-luc-bearing mice to further verify the targeting and penetration capacity. In a full-field image of brain tissues by fluorescence microscopy imaging system BZ-X800E, a high abundance of AMD-5.8 MPa was observed accumulation in the whole glioma tissues, while they were rarely observed in the normal brain tissues, indicating excellent tumor targeting and permeation capacity (Figure 5B). Similarly, TEM images also indicated that AMD-5.8 MPa has an excellent ability to cross BBB/BBTB and penetrate into tumors in the brains of intracranial GL261-luc bearing mice (Figure 5C; Figure S34B, Supporting Information). Furthermore, we used a laser scanning confocal microscope and TEM to assess the ability of adaptive microdrugs (AMD-5.8 MPa) to cross BBB/BBTB and intratumor distribution post-intravenous administration in intracranial GL261-bearing mice at different times. As shown in Figure S34A (Supporting Information), at 0.5 h, a significant portion of the cy5-labeled AMD-5.8 MPa (purple) was observed in the tumor blood vessels (green, marked with CD34). However, some of these particles were also seen to be extravasating from the tumor blood vessel into the tumor tissues, indicating that there is an active crossing of BBB/BBTB and penetrating brain tumor tissue. With the extension of time, more and more cy5-labeled AMD-5.8 MPa were observed to be distributed in the glioma tissues. The efficient BBB/BBTB crossing and penetration capacities of AMD-5.8 MPa should be associated with their good transcytosis. Previous studies have demonstrated that transcytosis is associated with caveolin-mediated endocytosis.<sup>[51]</sup> Our experiments showed that the cellular uptake of AMD-103 kPa, AMD-5.8 MPa, and AMD-15.4 MPa mainly proceeded with caveolin-mediated endocytosis in GL261 cells (Figure S10, Supporting Information). Therefore, we investigated the transcytosis ability of adaptive microdrugs from GL261 cells to GL261 cells using DOX as a control by flow cytometry (Figures S35 and S36, Supporting Information).<sup>[52]</sup> The GL261 cells (A cells, red subpopulation) were co-incubated with adaptive microdrugs for 4 h. Following this, the culture medium of the GL261 cells (A cells, red subpopulation) was replaced and Hoechst33342-stained GL261



cells (B cells, orange and blue subpopulation) were introduced and co-incubated for an additional 1.5 h. Flow cytometry detected dual-fluorescent channels (PE/DOX and V450/Hoechst33342) and the cells with PE+V450+ (blue subpopulation) were gated to their transcytosis efficiency. First, we compared the transcytosis capability of adaptive microdrugs with or without c(RGDyK)-modification. The results indicated that the adaptive microdrugs (with c(RGDyK)-modification) exhibited better transcytosis effects than those of adaptive microdrugs (without c(RGDyK)-modification), suggesting that receptor-mediated endocytosis could enhance their transcytosis efficiency.<sup>[53,54]</sup> In particular, AMD-5.8 MPa (with c(RGDyK)-modification) presented the best transcytosis efficiency (Figure 5D). Furthermore, we compared the transcytosis capabilities of adaptive nanodrugs and microdrugs. The results indicated that adaptive microdrugs exhibited superior transcytosis capacity compared to their adaptive nanodrugs. Notably, the AMD-0.8  $\mu\text{m}$  variant exhibited an even greater transcytosis ability (Figure S37, Supporting Information). These results demonstrated that the obtained adaptive microdrugs, especially the AMD-5.8 MPa, exhibited excellent capacities for crossing BBB/BBTB, tumor targeting, and transcytosis, allowing effective accumulation and deep permeation in glioma tissues, which is beneficial to improve the antitumor efficacy.

#### 2.3.4. The Antitumor Efficacy of Three Kinds of Adaptive Microdrugs with Different Viscoelasticity In Vivo

Next, we assessed the antitumor efficacy of PBS, DOX, AMD-0.8  $\mu\text{m}$ , and the obtained adaptive microdrugs (AMD-103 kPa, AMD-5.8 MPa, and AMD-15.4 MPa) in intracranial GL261-luc xenograft mice. The results indicated that the AMD-5.8 MPa group presented the best anti-glioma efficacy in comparison with the other treatment groups (Figure 5E). In the overall survival analysis, the AMD-5.8 MPa group presented the best median survival, compared with the other treatment groups (Figure 5F). The order of median survival time was as follows: AMD-5.8 MPa (66.5 d) > AMD-15.4 MPa (48 d) > AMD-103 kPa (40 d) > DOX (29.5 d) > AMs (24.5 d) and PBS (24 d). The body weights of mice in the treatment groups are shown in Figure S38 (Supporting Information). Furthermore, we performed immunohistochemical analyses of Ki67 and CD34, which are markers of cell proliferation and endothelial-lined blood vessels, respectively (Figure S39, Supporting Information). The expression levels of Ki67 and CD34 in each group were: PBS > DOX > AMD-103 kPa > AMD-15.4 MPa > AMD-5.8 MPa. Similar results were obtained in an

intracranial LN229-luc xenograft mice model (Figure S40, Supporting Information). Moreover, the biochemical indicators (alanine aminotransferase (ALT), aspartate aminotransferase (AST), blood urea nitrogen (BUN), and creatinine (Cre)) related to liver and kidney function in the adaptive microdrugs presented similar level as control (Figure S41, Supporting Information). In addition, we did not observe the damaged tissue in major organs in the treatment groups, suggesting the good biosafety and biocompatibility of these adaptive microdrugs for glioma treatment in vivo (Figure S42, Supporting Information).

In discussion, the aforementioned results indicated that these adaptive drug particles, particularly the microdrugs, had great potential to cross BBB/BBTB by enhanced interfacial binding and endocytosis via adaptive deformation. In addition, the integrity of the BBB may be compromised during glioma progression, resulting in a leaky BBB.<sup>[55,56]</sup> This condition may potentially facilitate the passage of the drug particles across the BBB via leakage.<sup>[57]</sup> Meanwhile, the degrees of BBB leakage in different glioma models (such as transplanted models, virus- or drug-induced models) may be different.<sup>[58,59]</sup> As such, the degrees of leaky BBB may also affect the crossing capacity of the drug delivery system, although the parallel comparison analysis and underlying mechanisms in different glioma models remain not well-explored. And, previous reports have proved that nanodrugs, with sizes ranging from 20 to 70 nm, are more effective in crossing and leaking the BBB into glioma microenvironments compared to particles of other sizes.<sup>[9–11]</sup> In our study, although the leaky BBB is possible, we parallelly compared the capacity of different groups in crossing BBB/BBTB, including the adaptive microdrugs, adaptive nanodrugs and free small molecule DOX. The results suggested that bioinspired adaptive microdrugs exhibited enhanced efficiency in crossing the BBB/BBTB compared to their adaptive nanodrugs and free DOX. Therefore, beyond the drug delivery by leaky BBB, the adaptive deformation-enhanced receptor-ligand-interfacial binding and endocytosis should be the main contributions to the enhancement of BBB/BBTB crossing and tumor tissue penetration of adaptive microdrugs.

### 3. Conclusion

In summary, we developed bioinspired adaptive microdrugs for enhanced chemotherapy of malignant glioma. The bioinspired micro-sized adaptive microdrugs were more efficient than nano-sized nanodrugs in crossing the BBB/BBTB, allowing more drugs to be delivered into tumor tissues. When they crossed

**Figure 5.** The biological activities of the three kinds of adaptive microdrugs with different viscoelasticities in vivo. A) DOX accumulation in tumors of GL261 glioma-bearing mice at different times treated with DOX, AMD-103 kPa, AMD-5.8 MPa, and AMD-15.4 MPa (equal with DOX concentration 2.5 mg kg<sup>-1</sup>) after administration via tail vein. B) Fluorescence microscopy images of the distribution of adaptive microdrugs (AMD-5.8 MPa) into tumor tissues of GL261-luc bearing glioma mice after intravenous injection. The nucleus was stained by Hoechst 33342 and the red signal represented DOX. T denotes tumor tissues and N denotes normal tissues. Scale bars in images from left to right: 2 cm, 100  $\mu\text{m}$ , and 50  $\mu\text{m}$ . In a full-field image of brain tissues by fluorescence microscopy imaging system BZ-X800E, high abundance of AMD-5.8 MPa was observed accumulation in the whole glioma tissues (T), while they were rarely observed in the normal brain tissues (N), indicating excellent tumor targeting and permeation capacity. C) TEM images of the AMD-5.8 MPa crossing BBB/BBTB and accumulation in glioma tissues. Scale bars in images from left to right: 1  $\mu\text{m}$ , 2  $\mu\text{m}$ , and 500 nm. D) The transcytosis efficiency of DOX, c(RGDyK)-modified AMD-103 kPa, AMD-5.8 MPa, and AMD-15.4 MPa from GL261 cells to GL261 cells determined by PE+/V450+ of flow cytometry. A cells: GL261 cells, red subpopulation. B cells: Hoechst33342-stained GL261 cells. The subpopulation cells of PE+/V450+ (blue color) represented transcytosis efficiency. E) IVIS bioluminescent images of representative glioma-luc-bearing mice from each treatment group at different times. F) The bioluminescent signal intensity curve of each treatment group ( $n = 6$ ). Normalized to 0 days of glioma-luc-bearing mice in all groups. G) Kaplan–Meier survival curves of the mice in each treatment group. Results are represented as mean  $\pm$  SD ( $n = 6$ ), \* $P < 0.05$ , \*\* $P < 0.01$ , \*\*\* $P < 0.001$ .

the BBB/BBTB, they were able to experience adaptive deformation to increase receptor-ligand-interfacial binding and endocytosis, significantly enhancing the drug accumulation, deep penetration, and cellular internalization into tumor tissues in comparison with their nanodrugs and thereby promoting the survival rates of glioblastoma mice. Therefore, we may conclude that the adaptive deformation capacity of bioinspired adaptive microdrugs enabled them to further amplify their interfacial interaction with cells (such as endothelial cells and tumor cells). This was achieved through an increase in contact interfaces between adaptive microdrugs and cells as a result of adaptive deformation, and thereby amplifying the receptor-ligand-interfacial binding and endocytosis. As a result, there was a significant improvement in the crossing of BBB/BBTB and downstream chemotherapy efficiency of malignant glioma. We strongly believe that the bioinspired adaptive microdrugs provide important clues for designing more efficient drug delivery systems by utilizing adaptive deformation to regulate the interfacial interactions, which would be utilized to enhance the therapeutic efficacy of solid tumors.<sup>[60]</sup>

## 4. Experimental Section

Experimental details are included in the Supporting Information.

## Supporting Information

Supporting Information is available from the Wiley Online Library or from the author.

## Acknowledgements

This work was supported by the National Key R&D Programme of China (2022YFA0806301); the National Natural Science Foundation of China (22275080 and 22075127); Guangdong Basic and Applied Basic Research Foundation (2022A1515012044); and Science and Technology Program of Guangzhou (2024A04J6606 and 2024B03J0001).

## Conflict of Interest

The authors declare no conflict of interest.

## Data Availability Statement

The data that support the findings of this study are available from the corresponding author upon reasonable request.

## Keywords

adaptive microdrugs, bioinspired materials, deformation, drug delivery, glioblastoma chemotherapy

Received: April 10, 2024  
Revised: May 13, 2024  
Published online: June 16, 2024

[1] Y. Wang, Y. Jiang, D. Wei, P. Singh, Y. Yu, T. Lee, L. Zhang, H. K. Mandl, A. S. Piotrowski-Daspit, X. Chen, F. Li, X. Li, Y. Cheng, A. Josowitz, F.

- Yang, Y. Zhao, F. Wang, Z. Zhao, A. Huttner, R. S. Bindra, H. Xiao, W. Mark Saltzman, *Nat. Biomed. Eng.* **2021**, *5*, 1048.
- [2] T. S. van Solinge, L. Nieland, E. A. Chiocca, M. L. D. Broekman, *Nat. Rev. Neurol.* **2022**, *18*, 221.
- [3] A. F. Eichler, E. Chung, D. P. Kodack, J. S. Loeffler, D. Fukumura, R. K. Jain, *Nat. Rev. Clin. Oncol.* **2011**, *8*, 344.
- [4] C. D. Arvanitis, G. B. Ferraro, R. K. Jain, *Nat. Rev. Cancer* **2020**, *20*, 26.
- [5] W. Zhang, A. Mehta, Z. Tong, L. Esser, N. H. Voelcker, *Adv. Sci.* **2021**, *8*, 2003937.
- [6] W. Tang, W. Fan, J. Lau, L. Deng, Z. Shen, X. Chen, *Chem. Soc. Rev.* **2019**, *48*, 2967.
- [7] J. Xie, Z. Shen, Y. Anraku, K. Kataoka, X. Chen, *Biomaterials* **2019**, *224*, 119491.
- [8] J. Li, J. Zhao, T. Tan, M. Liu, Z. Zeng, Y. Zeng, L. Zhang, C. Fu, D. Chen, T. Xie, *Int. J. Nanomed.* **2020**, *15*, 2563.
- [9] H. Wu, H. Lu, W. Xiao, J. Yang, H. Du, Y. Shen, H. Qu, B. Jia, S. K. Manna, M. Ramachandran, X. Xue, Z. Ma, X. Xu, Z. Wang, Y. He, K. S. Lam, R. J. Zawadzki, Y. Li, T. Y. Lin, *Adv. Mater.* **2020**, *32*, 1903759.
- [10] L. J. Cruz, M. A. Stammes, I. Que, E. R. van Beek, V. T. Knol-Blanckevoort, T. J. A. Snoeks, A. Chan, E. L. Kaijzel, C. Löwik, *J. Controlled Release* **2016**, *223*, 31.
- [11] J. Zhou, T. R. Patel, R. W. Sirianni, G. Strohbehn, M. Q. Zheng, N. Duong, T. Schafbauer, A. J. Huttner, Y. Huang, R. E. Carson, Y. Zhang, D. J. Sullivan Jr., J. M. Piepmeier, W. M. Saltzman, *Proc. Natl. Acad. Sci. USA* **2013**, *110*, 11751.
- [12] W. Niu, Q. Xiao, X. Wang, J. Zhu, J. Li, X. Liang, Y. Peng, C. Wu, R. Lu, Y. Pan, J. Luo, X. Zhong, H. He, Z. Rong, J. B. Fan, Y. Wang, *Nano Lett.* **2021**, *21*, 1484.
- [13] Y. Jiang, W. Yang, J. Zhang, F. Meng, Z. Zhong, *Adv. Mater.* **2018**, *30*, 1800316.
- [14] T. Lin, P. Zhao, Y. Jiang, Y. Tang, H. Jin, Z. Pan, H. He, V. C. Yang, Y. Huang, *ACS Nano* **2016**, *10*, 9999.
- [15] J. S. Michael, B. S. Lee, M. Zhang, J. S. Yu, *J. Transl. Int. Med.* **2018**, *6*, 128.
- [16] S. Sindhwani, A. M. Syed, J. Ngai, B. R. Kingston, L. Maiorino, J. Rothschild, P. MacMillan, Y. Zhang, N. U. Rajesh, T. Hoang, J. L. Y. Wu, S. Wilhelm, A. Zilman, S. Gadde, A. Sulaiman, B. Ouyang, Z. Lin, L. Wang, M. Egeblad, W. C. W. Chan, *Nat. Mater.* **2020**, *19*, 566.
- [17] S. Pandit, D. Dutta, S. Nie, *Nat. Mater.* **2020**, *19*, 478.
- [18] B. Ouyang, W. Poon, Y. N. Zhang, Z. P. Lin, B. R. Kingston, A. J. Tavares, Y. Zhang, J. Chen, M. S. Valic, A. M. Syed, P. MacMillan, J. Couture-Sénécal, G. Zheng, W. C. W. Chan, *Nat. Mater.* **2020**, *19*, 1362.
- [19] C. D. Arvanitis, G. B. Ferraro, R. K. Jain, *Nat. Rev. Cancer* **2020**, *20*, 26.
- [20] R. Skalak, P. I. Branemark, *Science* **1969**, *164*, 717.
- [21] T. Worbs, S. I. Hammerschmidt, R. Förster, *Nat. Rev. Immunol.* **2017**, *17*, 30.
- [22] F. Gaertner, Z. Ahmad, G. Rosenberger, S. Fan, L. Nicolai, B. Busch, G. Yavuz, M. Luckner, H. Ishikawa-Ankerhold, R. Hennel, A. Benechet, M. Lorenz, S. Chandraratne, I. Schubert, S. Helmer, B. Striednig, K. Stark, M. Janko, R. T. Böttcher, A. Verschoor, C. Leon, C. Gachet, T. Gudermann, Y. S. M. Mederos, Z. Pincus, M. Iannacone, R. Haas, G. Wanner, K. Lauber, M. Sixt, et al., *Cell* **2017**, *171*, 1368.
- [23] M. Diez-Silva, M. Dao, J. Han, C. T. Lim, S. Suresh, *MRS Bull.* **2010**, *35*, 382.
- [24] K. Ben M'Barek, D. Molino, S. Quignard, M. A. Plamont, Y. Chen, P. Chavrier, J. Fattaccioli, *Biomaterials* **2015**, *51*, 270.
- [25] Y. Xia, J. Wu, W. Wei, Y. Du, T. Wan, X. Ma, W. An, A. Guo, C. Miao, H. Yue, S. Li, X. Cao, Z. Su, G. Ma, *Nat. Mater.* **2018**, *17*, 187.
- [26] L. L. Pontani, I. Jorjadze, V. Viasnoff, J. Brujic, *Proc. Natl. Acad. Sci. USA* **2012**, *109*, 9839.
- [27] K. Y. Lee, D. J. Mooney, *Prog. Polym. Sci.* **2012**, *37*, 106.
- [28] C. Wang, T. Yokota, T. Someya, *Chem. Rev.* **2021**, *121*, 2109.
- [29] E. Ruvinov, S. Cohen, *Adv. Drug Delivery Rev.* **2016**, *96*, 54.

- [30] G. Muñoz Taboada, P. Dosta, E. R. Edelman, N. Artzi, *Adv. Mater.* **2022**, *34*, 2203087.
- [31] L. Sun, J. E. Zhou, T. Luo, J. Wang, L. Kang, Y. Wang, S. Luo, Z. Wang, Z. Zhou, J. Zhu, J. Yu, L. Yu, Z. Yan, *Adv. Mater.* **2022**, *34*, 2109969.
- [32] Z. Cong, S. Tang, L. Xie, M. Yang, Y. Li, D. Lu, J. Li, Q. Yang, Q. Chen, Z. Zhang, X. Zhang, S. Wu, *Adv. Mater.* **2022**, *34*, 2201042.
- [33] Q. Xiao, W. Zhao, C. Wu, X. Wang, J. Chen, X. Shi, S. Sha, J. Li, X. Liang, Y. Yang, H. Guo, Y. Wang, J. B. Fan, *Adv. Sci.* **2022**, *9*, 2105274.
- [34] R. Lu, X. Shi, Y. Pan, J. Li, Z. Liu, Q. Xiao, X. Wang, J. Chen, X. Zhang, J. Meng, W. Zhao, Y. Wang, J. B. Fan, *Adv. Ther.* **2022**, *6*, 2200131.
- [35] J. Luo, X. Zhong, Y. Peng, C. Hao, X. Liang, Y. Yang, X. Shi, X. Chen, X. Yi, X. Li, J. Wu, J. Li, Q. Xiao, C. Wu, R. Lu, Y. Pan, X. Wang, J. B. Fan, Y. Wang, Y. Wang, *Bioact Mater* **2022**, *13*, 179.
- [36] S. Avinash, E. Manivannan, K. P. Suresh, D. Shipra, X. Zheng, T. Liu, S. Masayuki, M. Joseph, M. Janet, K. P. Ravindra, *Mol. Pharmaceutics* **2011**, *8*, 1186.
- [37] C. Fan, K. Xu, Y. Huang, S. Liu, T. Wang, W. Wang, W. Hu, L. Liu, M. Xing, S. Yang, *Bioact Mater* **2020**, *6*, 1150.
- [38] Y. Li, S. Chen, M. Zhang, X. Ma, J. Zhao, Y. Ji, *ACS Appl. Mater. Interfaces* **2024**, *16*, 2140.
- [39] L. Wang, Y. Hou, X. Zhong, J. Hu, F. Shi, H. Mi, *Carbohydr. Polym.* **2019**, *208*, 42.
- [40] X. Meng, W. Ha, C. Cheng, Q. Zhen, L. Ding, B. Li, S. Zhang, *Langmuir* **2011**, *27*, 14401.
- [41] L. Qiu, Q. Hu, L. Cheng, L. Li, C. Tian, W. Chen, Q. Chen, W. Hu, L. Xu, J. Yang, L. Cheng, D. Chen, *Acta Biomater.* **2016**, *30*, 285.
- [42] J. S. Basuki, H. T. Duong, A. Macmillan, R. B. Erlich, L. Esser, M. C. Akerfeldt, R. M. Whan, M. Kavallaris, C. Boyer, T. P. Davis, *ACS Nano* **2013**, *7*, 10175.
- [43] W. Xu, J. Ding, C. Xiao, L. Li, X. Zhuang, X. Chen, *Biomaterials* **2015**, *54*, 72.
- [44] X. Yi, H. Gao, *Nanoscale* **2017**, *9*, 454.
- [45] J. A. Eble, *J Vis Exp* **2018**, *132*, 57334.
- [46] W. Jiang, B. Y. Kim, J. T. Rutka, W. C. Chan, *Nat. Nanotechnol.* **2008**, *3*, 145.
- [47] Z. Shen, H. Ye, X. Yi, Y. Li, *ACS Nano* **2019**, *13*, 215.
- [48] K. A. Beningo, Y. L. Wang, *J. Cell Sci.* **2002**, *115*, 849.
- [49] A. C. Anselmo, M. Zhang, S. Kumar, D. R. Vogus, S. Menegatti, M. E. Helgeson, S. Mitragotri, *ACS Nano* **2015**, *9*, 3169.
- [50] Y. Hui, D. Wibowo, Y. Liu, R. Ran, H. F. Wang, A. Seth, A. P. J. Middelberg, C. X. Zhao, *ACS Nano* **2018**, *12*, 2846.
- [51] D. E. Tylawsky, H. Kiguchi, J. Vaynshteyn, J. Gerwin, J. Shah, T. Islam, J. A. Boyer, D. R. Boué, M. Snuderl, M. B. Greenblatt, Y. Shamay, G. P. Raju, D. A. Heller, *Nat. Mater.* **2023**, *22*, 391.
- [52] J. Chen, J. Pan, S. Liu, Y. Zhang, S. Sha, H. Guo, X. Wang, X. Hao, H. Zhou, S. Tao, Y. Wang, J. B. Fan, *Adv. Mater.* **2023**, *35*, 2304187.
- [53] J. C. Ullman, A. Arguello, J. A. Getz, A. Bhalla, C. S. Mahon, J. Wang, T. Giese, C. Bedard, D. J. Kim, J. R. Blumenfeld, N. Liang, R. Ravi, A. A. Nugent, S. S. Davis, C. Ha, J. Duque, H. L. Tran, R. C. Wells, S. Lianoglou, V. M. Daryani, W. Kwan, H. Solanoy, H. Nguyen, T. Earr, J. C. Dugas, M. D. Tuck, J. L. Harvey, M. L. Reyzer, R. M. Caprioli, S. Hall, S. Poda, P. E. Sanchez, M. S. Dennis, K. Gunasekaran, A. Srivastava, T. Sandmann, K. R. Henne, R. G. Thorne, G. Di Paolo, G. Astarita, D. Diaz, A. P. Silverman, R. J. Watts, Z. K. Sweeney, M. S. Kariolis, A. G. Henry, *Sci. Transl. Med.* **2020**, *12*, 1163.
- [54] H. J. Liu, P. Xu, *Adv. Drug Delivery Rev.* **2022**, *191*, 114619.
- [55] C. D. Arvanitis, G. B. Ferraro, R. K. Jain, *Nat. Rev. Cancer* **2020**, *20*, 26.
- [56] A. F. Eichler, E. Chung, D. P. Kodack, J. S. Loeffler, D. Fukumura, R. K. Jain, *Nat. Rev. Clin. Oncol.* **2011**, *8*, 344.
- [57] J. Li, M. Zheng, O. Shimoni, W. A. Banks, A. I. Bush, J. R. Gamble, B. Shi, *Adv. Sci.* **2021**, *8*, e2101090.
- [58] D. R. Groothuis, J. M. Fischer, G. Lapin, D. D. Bigner, N. A. Vick, *J Neuropathol Exp Neurol* **1982**, *41*, 164.
- [59] D. R. Groothuis, J. M. Fischer, N. A. Vick, D. D. Bigner, *Cancer Treat Rep* **1981**, *65*, 13.
- [60] S. Tao, B. Lin, H. Zhou, S. Sha, X. Hao, X. Wang, J. Chen, Y. Zhang, J. Pan, J. Xu, J. Zeng, Y. W., X. He, J. Huang, W. Zhao, J. B. Fan, *Nat. Commun.* **2023**, *14*, 5575.